

A lowest order stabilization-free mixed Virtual Element Method

Original

A lowest order stabilization-free mixed Virtual Element Method / Borio, Andrea; Lovadina, Carlo; Marcon, Francesca; Visinoni, Michele. - In: COMPUTERS & MATHEMATICS WITH APPLICATIONS. - ISSN 0898-1221. - ELETTRONICO. - 160:(2024), pp. 161-170. [10.1016/j.camwa.2024.02.024]

Availability:

This version is available at: 11583/2986478 since: 2024-03-01T09:20:39Z

Publisher:

Elsevier

Published

DOI:10.1016/j.camwa.2024.02.024

Terms of use:

This article is made available under terms and conditions as specified in the corresponding bibliographic description in the repository

Publisher copyright

Elsevier postprint/Author's Accepted Manuscript

© 2024. This manuscript version is made available under the CC-BY-NC-ND 4.0 license
<http://creativecommons.org/licenses/by-nc-nd/4.0/>. The final authenticated version is available online at:
<http://dx.doi.org/10.1016/j.camwa.2024.02.024>

(Article begins on next page)

A lowest order stabilization-free mixed Virtual Element Method

Andrea Borio^{a,1}, Carlo Lovadina^{b,c,1}, Francesca Marcon^{a,1}, Michele Visinoni^{b,1,*}

^a*Dipartimento di Scienze Matematiche, Politecnico di Torino, Corso Duca degli Abruzzi 24, Torino, 10129, Italy*

^b*Dipartimento di Matematica, Università degli studi di Milano, Via Saldini 50, Milano, 20133, Italy*

^c*IMATI-CNR, Via Ferrata 5, Pavia, 27100, Italy*

Abstract

We initiate the design and the analysis of stabilization-free Virtual Element Methods for the Poisson problem written in mixed form. A Virtual Element version of the lowest order Raviart-Thomas Finite Element is considered. To reduce the computational costs, a suitable projection on the gradients of harmonic polynomials is employed. A complete theoretical analysis of stability and convergence is developed in the case of quadrilateral meshes. Some numerical tests highlighting the actual behaviour of the scheme are also provided.

Keywords: Virtual element method, Mixed formulation, Quadrilateral meshes, Poisson problem

2020 MSC: 65N12, 65N30

1. Introduction

2 In these years, the study of numerical methods for solving partial dif-
3 ferential equations on polygonal/polytopal meshes has been experiencing

*Corresponding author

Email addresses: andrea.borio@polito.it (Andrea Borio),
carlo.lovadina@unimi.it (Carlo Lovadina), francesca.marcon@polito.it
(Francesca Marcon), michele.visinoni@unimi.it (Michele Visinoni)

¹The authors are members of the INdAM-GNCS.

4 a growing interest in the scientific community. In particular, one of the
5 most recent developments in this field is represented by the Virtual Element
6 Method (VEM). This technology was first introduced for the primal con-
7 forming Poisson problem in [1] as a generalization of H^1 -conforming Finite
8 Element Method. Successively, the extension to the $H(\text{div})$ -conforming vec-
9 tor fields, generalizing Mixed Finite Elements [2], has been introduced in [3]
10 and developed in [4, 5, 6]. Thanks to the great flexibility of the method,
11 both the primal and the mixed formulation of VEM have been applied to a
12 large range of applications, such as elastic and inelastic problems [7, 8, 9, 10],
13 simulations in fractured media [11, 12, 13, 14] and in porous media mechanics
14 [15, 16, 17], just to mention a few of them.

15 The key ideas of VEM may be summarised as follows.

- 16 • The local approximation spaces are defined as the solutions to suitable
17 local partial differential problems. Therefore, VEM functions are not
18 explicitly known, but only a limited information is available. However,
19 the local approximation spaces contain polynomials up to a suitable
20 degree.
- 21 • A computable projection onto a polynomial space is involved. Typi-
22 cally, the projection is evaluated onto the polynomials contained in the
23 approximation spaces.
- 24 • The discrete bilinear forms are characterized by the sum of a singular
25 part maintaining consistency on polynomials, and a stabilizing form
26 enforcing coercivity.

27 However, in general the stabilising form mentioned above is designed
28 without a clear physical meaning, but only requiring minimal assumptions
29 to make the method stable. Though efficient recipes to tune the stabilisation
30 term have been proposed (see for instance [18, 19]), in certain complex situ-
31 ations it might be preferable to avoid dealing with the choice of such forms.
32 As examples, we mention highly non-linear problems; problems where highly
33 anisotropic meshes occurs; advection-diffusion problems. In addition, the
34 stabilization term could be problematic in connection with the analysis of
35 a-posteriori error estimates [20, 21] (however, the recent work [22] presents
36 a first study which provides stabilization-free upper and lower a-posteriori
37 bounds for triangular meshes with hanging nodes).

38 Virtual Element schemes for which no stabilisation form is required have
39 been recently presented, in different 2D frameworks, in [23, 24, 25, 26, 27, 28].
40 These approaches share the idea to employ a projection onto a polynomial
41 space of higher degree than the one usually taken in standard VEM. It is
42 worth noticing that the polynomial degree depends on the number of edges
43 of each polygon: as expected, it increases as the edge number gets larger.
44 As a consequence, the quadrature computational cost significantly grows in
45 presence of elements with many edges, without any improvement in the con-
46 vergence rate.

47 This paper follows similar lines of the above-mentioned stabilisation-free
48 attempts [23, 24, 25, 26, 27, 28], but for the Poisson problem written in the
49 usual $H(\text{div}) - L^2$ mixed formulation. In particular, we consider a VEM ver-
50 sion of the lowest order Raviart-Thomas Finite Element Method, see [4]. To
51 reduce the computational cost connected to quadrature, a suitable projection
52 operator onto the gradients of *harmonic* polynomials is selected, similarly to
53 the scheme introduced for the primal formulation in [29]. The resulting
54 scheme has the following features.

- 55 • It is a conforming mixed VEM method for which no stabilization term
56 is needed.
- 57 • The method shows first order convergence rate for the natural norms
58 and, in most cases, a behaviour comparable with the standard lowest
59 order Raviart-Thomas VEM for which the stabilisation term is suitably
60 tuned. However, for highly anisotropic meshes, our method seems to
61 display a better performance.
- 62 • Despite a projection over higher-order polynomial spaces is employed,
63 the use of *harmonic* polynomials greatly alleviate the additional com-
64 putational costs.

65 These properties indicate that the present approach could be a valid alterna-
66 tive to the lowest order Raviart-Thomas Virtual Element Methods, especially
67 in those complex situations where, for the latter scheme, a particular care in
68 the treatment of the stabilising form is required.

69 From a theoretical point of view, the present paper can be considered as
70 a first contribution, since we present a rigorous analysis only for the quadri-
71 lateral case. Of course, similar and simpler arguments could be applied also
72 for triangular elements. For such a case, there is no need to introduce the

73 Hourglass space $H(E)$, see (27), since the flux variable is locally approxi-
74 mated only by means of the standard lowest-order Raviart-Thomas Finite
75 Element $RT_0(E)$, see (26). However, the general theory for polygons with an
76 arbitrary number of edges is not currently available and will be treated in a
77 future work.

78 A brief outline of the paper is as follows. In Section 2 we define the
79 model problem. Section 3 contains the statement of the discrete problems,
80 introducing all the bilinear and linear forms involved. In section 4, we prove
81 the well-posedness of the discrete problem in the quadrilateral case. For
82 the same kind of meshes, we derive optimal error estimates in Section 5
83 and, finally, in Section 6 we present some numerical results that assess the
84 convergence rate of the method; a comparison with the standard lowest order
85 Raviart-Thomas VEM is also provided.

86 2. Model problem

87 Let $\Omega \subset \mathbb{R}^2$ be a computational domain. We are interested in studying
88 the following mixed formulation of the Poisson problem:

$$\begin{cases} -\operatorname{div} \boldsymbol{\sigma} = f & \text{in } \Omega \\ \boldsymbol{\sigma} = \nabla u & \text{in } \Omega \\ u = 0 & \text{on } \partial\Omega, \end{cases} \quad (1)$$

89 where the forcing term $f \in L^2(\Omega)$. We consider homogeneous natural bound-
90 ary conditions only for sake of simplicity. The extension to non-homogeneous
91 or essential boundary conditions can be treated with the same techniques
92 used for other more classical Galerkin methods, such as the FEM. Let $(\cdot, \cdot)_\Omega$
93 denote the L^2 scalar product and $a(\boldsymbol{\sigma}, \boldsymbol{\tau}) := (\boldsymbol{\sigma}, \boldsymbol{\tau})_\Omega$. Then the mixed vari-
94 ational formulation of (1) is given by: find $(\boldsymbol{\sigma}, u) \in \Sigma \times U$, where $\Sigma :=$
95 $H(\operatorname{div}, \Omega)$ and $U := L^2(\Omega)$ such that

$$\begin{cases} a(\boldsymbol{\sigma}, \boldsymbol{\tau}) + (\operatorname{div} \boldsymbol{\tau}, u)_\Omega = 0 & \forall \boldsymbol{\tau} \in \Sigma, \\ (\operatorname{div} \boldsymbol{\sigma}, v)_\Omega = -(f, v)_\Omega & \forall v \in U. \end{cases} \quad (2)$$

96 Well posedness of the above problem (2) is standard and the details can be
97 found, for instance, in [2].

98 **3. VEM discrete formulation**

99 In order to state the discrete formulation of (2), let \mathcal{M}_h be a polygonal
100 tessellation of Ω . For every element $E \in \mathcal{M}_h$, its area and diameter are
101 denoted by $|E|$ and h_E , respectively. As usual, the maximum of the diameters
102 h_E for $E \in \mathcal{M}_h$ is the mesh size, denoted by h , i.e. $h = \max_{E \in \mathcal{M}_h} h_E$. We
103 assume that each $E \in \mathcal{M}_h$ is such that

104 **A.1** E is star-shaped with respect to a ball of radius $\geq \gamma h_E$,

105 **A.2** for any edge e of ∂E , $|e| \geq \gamma h_E$,

106 where γ is a positive constant. To continue, for any given $E \in \mathcal{M}_h$ and
107 non-negative integer k , $\mathbb{P}_k(E)$ denotes the space of polynomials of degree up
108 to k defined on E . Moreover, we introduce $\mathbb{P}_k^H(E) \subseteq \mathbb{P}_k(E)$ as the space of
109 *harmonic* polynomials of degree up to k defined on E ; the dimension of this
110 latter space is $2k + 1$.

111 *3.1. The local spaces*

112 In this section we introduce the discrete local spaces and their interpola-
113 tion properties. Given an element $E \in \mathcal{M}_h$, we introduce the following local
114 VEM space:

$$\begin{aligned} \Sigma_h(E) := \{ \boldsymbol{\tau}_h \in \mathbf{H}(\operatorname{div}, E) : \exists v \in \mathbf{H}^1(E) \text{ s.t. } \boldsymbol{\tau}_h = \nabla v, \\ \boldsymbol{\tau}_h \cdot \mathbf{n}_e \in \mathbb{P}_0(e) \quad \forall e \in \partial E, \quad \operatorname{div} \boldsymbol{\tau}_h \in \mathbb{P}_0(E) \}. \end{aligned} \quad (3)$$

115 Accordingly, for the local space $\Sigma_h(E)$ the following degrees of freedom can
116 be taken:

$$\boldsymbol{\tau}_h \rightarrow \frac{1}{|e|} \int_e \boldsymbol{\tau}_h \cdot \mathbf{n}_e \, de = \boldsymbol{\tau}_h \cdot \mathbf{n}_e \quad \forall e \in \partial E. \quad (4)$$

117 The unisolvence of the above degrees of freedom is proved, e.g., as in [5], so
118 that $\dim(\Sigma_h(E)) = n_E$, where n_E is the edge number of E . We remark that,
119 once $\boldsymbol{\tau}_h \cdot \mathbf{n}_e = c_e \in \mathbb{P}_0(E)$ is given for all $e \in \partial E$, the quantity $\operatorname{div} \boldsymbol{\tau}_h \in \mathbb{P}_0(E)$
120 is uniquely determined. Since $\operatorname{div} \boldsymbol{\tau}_h \in \mathbb{P}_0(E)$ then

$$\operatorname{div} \boldsymbol{\tau}_h = \frac{1}{|E|} \int_E \operatorname{div} \boldsymbol{\tau}_h \, dE = \frac{1}{|E|} \sum_{e \in \partial E} \int_e \boldsymbol{\tau}_h \cdot \mathbf{n}_e \, de = \frac{1}{|E|} \sum_{e \in \partial E} |e| c_e. \quad (5)$$

121 The local approximation space for U is simply defined as follows

$$U_h(E) := \{ u_h \in L^2(E) : u_h \in \mathbb{P}_0(E) \}. \quad (6)$$

122 Accordingly, for the local space $U_h(E)$ the following degrees of freedom can
 123 be taken:

$$u_h \rightarrow \frac{1}{|E|} \int_E u_h \, dE. \quad (7)$$

124 It follows that $\dim(U_h(E)) = 1$.

125 3.2. Approximation in Σ_h and U_h

126 Let us consider the space $W(\Omega) = H(\operatorname{div}, \Omega) \cap [L^r(\Omega)]^2$ ($r > 2$), equipped
 127 with the natural norm. We define an interpolation operator

$$\mathcal{I}_h : W(\Omega) \longrightarrow \Sigma_h \quad (8)$$

128 by requiring

$$\int_e (\boldsymbol{\varsigma} - \mathcal{I}_h \boldsymbol{\varsigma}) \cdot \mathbf{n}_e \, de = 0, \quad \forall \text{ edge } e \text{ of the elements in } \mathcal{M}_h. \quad (9)$$

129 Using the unisolvence of the degrees of freedom, e.g. see [5], it is not difficult
 130 to check that such a $\mathcal{I}_h \boldsymbol{\varsigma}$ exists and it is unique in Σ_h . This definition implies
 131 that for each $E \in \mathcal{M}_h$

$$\int_E \operatorname{div} (\boldsymbol{\varsigma} - \mathcal{I}_h \boldsymbol{\varsigma}) \, dE = 0. \quad (10)$$

132 Hence, since for each $E \in \mathcal{M}_h$ $\operatorname{div} \mathcal{I}_h \boldsymbol{\varsigma} \in \mathbb{P}_0(E)$, we obtain the *commuting*
 133 *diagram property*

$$\operatorname{div} \mathcal{I}_h \boldsymbol{\varsigma} = \Pi_{0,E}^0 \operatorname{div} \boldsymbol{\varsigma}, \quad (11)$$

134 where $\Pi_{0,E}^0 : L^2(E) \rightarrow \mathbb{P}_0(E)$ is the L^2 projection operator onto constants.
 135 We now remark that $(\mathcal{I}_h \boldsymbol{\varsigma})|_E = \nabla \varphi^*$, φ^* being the solution to the local
 136 (compatible) Neumann problem

$$\begin{cases} \Delta \varphi^* = \Pi_{0,E}^0 \operatorname{div} \boldsymbol{\varsigma} & \text{in } E \\ \nabla \varphi^* \cdot \mathbf{n}_e = \Pi_{0,e}^0 (\boldsymbol{\varsigma} \cdot \mathbf{n}_e) & \text{on every } e \text{ side of } \partial E, \end{cases} \quad (12)$$

137 where $\Pi_{0,e}^0$ denotes the L^2 projection operator onto the constant functions on
 138 e . Regularity results of elliptic problems and Sobolev embedding theorems
 139 show that there exists $r^* > 2$ such that for $r \in (2, r^*]$ it holds

$$\|\mathcal{I}_h \boldsymbol{\varsigma}\|_{0,E} \leq C_{r^*} \|\boldsymbol{\varsigma}\|_{W(E)}. \quad (13)$$

140 Moreover assuming $\boldsymbol{\varsigma} \in [\mathbf{H}^1(\Omega)]^2$ and $\operatorname{div} \boldsymbol{\varsigma} \in \mathbf{H}^1(\Omega)$, the following approxima-
 141 tion results hold true: for each h , for each $E \in \mathcal{M}_h$

$$\|\operatorname{div}(\boldsymbol{\varsigma} - \mathcal{I}_h \boldsymbol{\varsigma})\|_{0,E} \leq C_d h_E^s |\operatorname{div} \boldsymbol{\varsigma}|_{s,E}, \quad s = 0, 1 \quad (14)$$

142 and

$$\|\boldsymbol{\varsigma} - \mathcal{I}_h \boldsymbol{\varsigma}\|_{0,E} \leq C_\varsigma h_E |\boldsymbol{\varsigma}|_{1,E}. \quad (15)$$

143 Above, C_{r^*} , C_d and C_ς are positive constants depending only on the constant
 144 γ of the mesh assumptions **A.1** and **A.2**.

145 Moreover, we recall that, given $w \in \mathbf{H}^1(\Omega)$, for its L^2 projection $\Pi_{0,E}^0 w \in$
 146 U_h it holds for each h , for each $E \in \mathcal{M}_h$

$$\|w - \Pi_{0,E}^0 w\|_{0,E} \leq C h_E^s |w|_{s,E} \quad s = 0, 1, \quad (16)$$

147 where $C > 0$ depends only on the constant γ of the mesh assumptions **A.1**
 148 and **A.2**.

149 3.3. The local forms

150 In this section we introduce the VEM counterparts of the local forms
 151 associated with the continuous problem.

The local mixed term. Given $E \in \mathcal{M}_h$, we notice that the term

$$(\operatorname{div} \boldsymbol{\tau}_h, v_h)_E = \int_E v_h \operatorname{div} \boldsymbol{\tau}_h \, dE$$

152 is computable for every $\boldsymbol{\tau}_h \in \Sigma_h(E)$ and $v_h \in U_h(E)$ via the degrees of
 153 freedom. For this reason, we do not need to introduce any approximation of
 154 the continuous terms $(\operatorname{div} \boldsymbol{\tau}, u)$ and $(\operatorname{div} \boldsymbol{\sigma}, v)$ in problem (2).

The local bilinear form $a^E(\cdot, \cdot)$. The local bilinear form

$$a^E(\boldsymbol{\sigma}_h, \boldsymbol{\tau}_h) = \int_E \boldsymbol{\sigma}_h \cdot \boldsymbol{\tau}_h \, dE$$

155 is not computable for a general pair $(\boldsymbol{\sigma}_h, \boldsymbol{\tau}_h) \in \Sigma_h(E) \times \Sigma_h(E)$. Here, instead
 156 of using the standard VEM procedure (cf. [4]), we introduce a local self-
 157 stabilized discrete bilinear form. Let

$$\hat{\Pi}_{k-1,E}^0 : [\mathbf{L}^2(E)]^2 \rightarrow \nabla \mathbb{P}_k^H(E) \quad (17)$$

158 be the $L^2(E)$ -projection operator onto the space $\nabla\mathbb{P}_k^H(E)$, i.e. the space of
 159 gradients of *harmonic* polynomials of degree at most k , with $k \geq 1$. More
 160 precisely, $\hat{\Pi}_E^0$ is defined by the orthogonality condition: for each $\boldsymbol{\tau} \in [L^2(E)]^2$,
 161 it holds

$$\left(\hat{\Pi}_{k-1,E}^0 \boldsymbol{\tau}, \nabla p \right)_E = (\boldsymbol{\tau}, \nabla p)_E \quad \forall p \in \mathbb{P}_k^H(E). \quad (18)$$

162 In order to attain stability, the approximation of $a^E(\cdot, \cdot)$ depends on n_E , i.e.
 163 the number of edges of E . More precisely, $[\cdot]$ being the integer part, we select
 164

$$k = \left\lceil \frac{n_E + 1}{2} \right\rceil \quad (19)$$

165 (i.e. k is the smallest integer such that $2k \geq n_E$). We then use the corre-
 166 sponding projection $\hat{\Pi}_E^0$, see (17) and (18), to define

$$a_h^E(\boldsymbol{\sigma}_h, \boldsymbol{\tau}_h) = \left(\hat{\Pi}_{k-1,E}^0 \boldsymbol{\sigma}_h, \hat{\Pi}_{k-1,E}^0 \boldsymbol{\tau}_h \right)_E \quad \forall \boldsymbol{\sigma}_h, \boldsymbol{\tau}_h \in \Sigma_h(E). \quad (20)$$

167 **Remark 1.** *We remark that, although a rigorous analysis is still missing for*
 168 *general polygons, the numerical tests (see Section 6.1) seem to suggest that*
 169 *the choice (19) always leads to a stable scheme.*

170 **Remark 2.** *Given $\boldsymbol{\tau}_h \in \Sigma_h(E)$, to compute $\hat{\Pi}_{k-1,E}^0 \boldsymbol{\tau}_h$ one has solve, from*
 171 *(18) and integrating by parts:*

$$\left(\hat{\Pi}_{k-1,E}^0 \boldsymbol{\tau}_h, \nabla p \right)_E = -(\operatorname{div} \boldsymbol{\tau}_h, p)_E + \int_{\partial E} (\boldsymbol{\tau}_h \cdot \mathbf{n}) p \, de \quad \forall p \in \mathbb{P}_k^H(E), \quad (21)$$

which is clearly computable, as $\operatorname{div} \boldsymbol{\tau}_h$ is computable and constant. Moreover,
integrating by parts also the left-hand side and taking into account that the
involved polynomials are harmonic, one realizes that the integral over E can
be computed as an integral over ∂E . In fact, recalling (17), $\hat{\Pi}_{k-1,E}^0 \boldsymbol{\tau}_h = \nabla q$
for some $q \in \mathbb{P}_k^H(E)$. Hence, since q is harmonic, we have

$$\left(\hat{\Pi}_{k-1,E}^0 \boldsymbol{\tau}_h, \nabla p \right)_E = (\nabla q, \nabla p)_E = \int_{\partial E} (\nabla q \cdot \mathbf{n}) p \, de = \int_{\partial E} (\hat{\Pi}_{k-1,E}^0 \boldsymbol{\tau}_h \cdot \mathbf{n}) p \, de.$$

172 *Therefore, only 1D quadrature rules are required to compute the left-hand*
 173 *side of (21). Furthermore, since $\operatorname{div} \boldsymbol{\tau}_h$ is constant, the first term in the right-*
 174 *hand side requires only to evaluate the integral of a harmonic polynomial of*
 175 *degree at most k . Hence, the computation of $\hat{\Pi}_{k-1,E}^0 \boldsymbol{\tau}_h$ is not as cumbersome*
 176 *as it may appear at a first sight.*

The local right-hand side term. We split the right-hand side term on each quadrilateral and we have

$$(f, v_h)_E = \int_E f v_h \, dE.$$

Since $v_h \in U_h(E) = \mathbb{P}_0(E)$, we have that

$$(f, v_h) = \sum_{E \in \mathcal{M}_h} v_h \int_E f \, dE,$$

177 which is computable via quadrature rules for polygonal domains, see for
178 instance [30].

179 3.4. The discrete scheme

180 Starting from the local spaces and local terms introduced in the previous
181 sections, we can set the global self-stabilized problem. More specifically, we
182 introduce these two global approximation spaces, by gluing the local approx-
183 imation spaces, see (3) and (6):

$$\Sigma_h = \{ \boldsymbol{\tau}_h \in \mathbf{H}(\operatorname{div}, \Omega) : \boldsymbol{\tau}_{h|E} \in \Sigma_h(E), \quad \forall E \in \mathcal{M}_h \} \quad (22)$$

184 and

$$U_h = \{ u_h \in U : u_{h|E} \in U_h(E), \quad \forall E \in \mathcal{M}_h \}. \quad (23)$$

185 Now, given a local approximation of $a^E(\cdot, \cdot)$, see (20), $\forall \boldsymbol{\sigma}_h, \boldsymbol{\tau}_h \in \Sigma_h$ we set

$$a_h(\boldsymbol{\sigma}_h, \boldsymbol{\tau}_h) := \sum_{E \in \mathcal{M}_h} a_h^E(\boldsymbol{\sigma}_h, \boldsymbol{\tau}_h). \quad (24)$$

186 We can state the discrete problem as: find $(\boldsymbol{\sigma}_h, u_h) \in \Sigma_h \times U_h$ such that

$$\begin{cases} a_h(\boldsymbol{\sigma}_h, \boldsymbol{\tau}_h) + (\operatorname{div} \boldsymbol{\tau}_h, u_h)_\Omega = 0 & \forall \boldsymbol{\tau}_h \in \Sigma_h \\ (\operatorname{div} \boldsymbol{\sigma}_h, v_h)_\Omega = (f, v_h)_\Omega & \forall v_h \in U_h \end{cases}. \quad (25)$$

187 In the next section we focus on the well-posedness of this discrete scheme, in
188 the case of quadrilateral meshes, which requires in particular the coercivity-
189 on-the-kernel condition for the bilinear form $a_h(\cdot, \cdot)$ (also called *ellipticity-*
190 *on-the-kernel condition*).

207 **Definition 2** (Hourglass space $\mathsf{H}(E)$). Let $\boldsymbol{\xi} \in \Sigma_h(E)$ be the function such
 208 that

$$\boldsymbol{\xi} \cdot \mathbf{n}_j = \frac{(-1)^j}{|e_j|} \quad \forall j = 1, \dots, 4, \quad (27)$$

209 then we introduce the following one dimensional virtual space

$$\mathsf{H}(E) := \text{span}(\boldsymbol{\xi}). \quad (28)$$

210 Using the divergence theorem, it is straightforward to see that a function
 211 $\tilde{\boldsymbol{\tau}}_h \in \mathsf{H}(E)$ satisfies $\text{div } \tilde{\boldsymbol{\tau}}_h = 0$.

212 **Remark 3.** We notice that the two spaces above are two subspaces of $\Sigma_h(E)$.

213 **Proposition 1.** Let $\text{RT}_0(E)$ be the space defined in (26) and let $\mathsf{H}(E)$ be the
 214 space defined in (28), then

$$\Sigma_h(E) = \text{RT}_0(E) \oplus \mathsf{H}(E). \quad (29)$$

215 Moreover, let us define the local divergence-free subspace:

$$\Sigma_h^0(E) = \{\boldsymbol{\tau}_h \in \Sigma_h(E) : \text{div } \boldsymbol{\tau}_h = 0\}. \quad (30)$$

216 Then it holds

$$\Sigma_h^0(E) = (\mathbb{P}_0(E))^2 \oplus \mathsf{H}(E) \quad (31)$$

217 and the decomposition is L^2 -orthogonal.

218 *Proof.* Notice that, according to the dimension of $\text{RT}_0(E)$ and $\mathsf{H}(E)$, to get
 219 (29) we only have to prove that $\text{RT}_0(E) \cap \mathsf{H}(E) = \{\mathbf{0}\}$. Then, take $\boldsymbol{\tau}_h \in$
 220 $\text{RT}_0(E) \cap \mathsf{H}(E)$. Since $\boldsymbol{\tau}_h \in \mathsf{H}(E)$ we have $\boldsymbol{\tau}_h = \lambda \boldsymbol{\xi}$ for a suitable real number
 221 λ . By the definition of $\boldsymbol{\xi}$, we get $\text{div } \boldsymbol{\tau}_h = \lambda \text{div } \boldsymbol{\xi} = 0$. Since $\boldsymbol{\tau}_h \in \text{RT}_0(E)$,
 222 we thus infer $\boldsymbol{\tau}_h \in (\mathbb{P}_0(E))^2$. It follows that $\boldsymbol{\tau}_h = \nabla(\boldsymbol{\tau}_h \cdot \mathbf{x}) = \lambda \nabla(\boldsymbol{\xi} \cdot \mathbf{x})$. We
 223 have, using integration by parts and (27):

$$\|\boldsymbol{\tau}_h\|_{0,E}^2 = \lambda^2 (\boldsymbol{\xi}, \nabla(\boldsymbol{\xi} \cdot \mathbf{x}))_E = \lambda^2 \int_{\partial E} (\boldsymbol{\xi} \cdot \mathbf{n}_E) (\boldsymbol{\xi} \cdot \mathbf{x}) = \lambda^2 \sum_{i=1}^4 \int_{e_j} \frac{(-1)^j}{|e_j|} (\boldsymbol{\xi} \cdot \mathbf{x}). \quad (32)$$

224 Therefore, an application of the trapezoidal rule gives

$$\|\boldsymbol{\tau}_h\|_{0,E}^2 = \lambda^2 \boldsymbol{\xi} \cdot \left(\frac{1}{2} \sum_{j=1}^4 (-1)^j (V_j + V_{j+1}) \right) = 0, \quad (33)$$

225 i.e. $\boldsymbol{\tau}_h = \mathbf{0}$, and thus (29) is proved. Furthermore, decomposition (31) follows
 226 from a dimensional count, while the L^2 -orthogonality is simply (33). \square

227 **Lemma 1.** *Let $E \in \mathcal{M}_h$ and let $\boldsymbol{\xi}$ be the hourglass function defined on E by*
 228 *(27). Then $\exists C_\xi > 0$ independent of h_E such that*

$$\|\boldsymbol{\xi}\|_0 \leq C_\xi. \quad (34)$$

229 *Proof.* Since $\boldsymbol{\xi} \in \Sigma_h(E)$, by (3) $\exists v \in H^1(E)$ such that $\boldsymbol{\xi} = \nabla v$. It is clear
 230 that v is defined up to a constant, so we choose v such that $\int_E v = 0$. This
 231 implies that $\exists C > 0$ independent of h_E such that

$$\|v\|_0 \leq Ch_E \|\nabla v\|_0 = Ch_E \|\boldsymbol{\xi}\|_0, \quad (35)$$

232 by Poincaré's inequality. Moreover, since $\operatorname{div} \boldsymbol{\xi} = 0$, it holds $\Delta v = 0$. Then,
 233 by Green's theorem and a Cauchy-Schwarz inequality we have

$$\|\boldsymbol{\xi}\|_0^2 = (\boldsymbol{\xi}, \nabla v)_E = (\boldsymbol{\xi} \cdot \mathbf{n}, v)_{\partial E} \leq \|\boldsymbol{\xi} \cdot \mathbf{n}\|_{0, \partial E} \|v\|_{0, \partial E}. \quad (36)$$

234 We can apply a standard trace inequality to the last norm and obtain, by
 235 exploiting also (35),

$$\|v\|_{0, \partial E} \leq Ch_E^{\frac{1}{2}} (h_E^{-2} \|v\|_0^2 + \|\nabla v\|_0^2)^{\frac{1}{2}} \leq Ch_E^{\frac{1}{2}} \|\boldsymbol{\xi}\|_0. \quad (37)$$

236 On the other hand, an explicit computation exploiting the definition of $\boldsymbol{\xi}$
 237 given by (27) yields

$$\|\boldsymbol{\xi} \cdot \mathbf{n}\|_{0, \partial E}^2 = \sum_{j=1}^4 \int_{e_j} \left[\frac{(-1)^j}{|e_j|} \right]^2 = \sum_{j=1}^4 |e_j|^{-1} \leq 4\gamma^{-1} h_E^{-1}, \quad (38)$$

where the last inequality is obtained by exploiting the mesh assumption **A.2**.
 Using (37) and (38) into (36), we get

$$\|\boldsymbol{\xi}\|_0^2 \leq \|\boldsymbol{\xi} \cdot \mathbf{n}\|_{0, \partial E} \|v\|_{0, \partial E} \leq 2\gamma^{-\frac{1}{2}} h_E^{-\frac{1}{2}} \cdot Ch_E^{\frac{1}{2}} \|\boldsymbol{\xi}\|_0 \leq C \|\boldsymbol{\xi}\|_0,$$

238 which yields the thesis. \square

239 **Lemma 2.** *Under the mesh assumptions **A.1** and **A.2**, for every $E \in \mathcal{M}_h$,*
 240 *there exists a positive constant C_* , independent of h_E , such that*

$$\left\| \hat{\Pi}_{1,E}^0 \tilde{\boldsymbol{\tau}}_h \right\|_0 \geq C_* \|\tilde{\boldsymbol{\tau}}_h\|_0 \quad \forall \tilde{\boldsymbol{\tau}}_h \in H(E). \quad (39)$$

241 *Proof.* Since $H(E) = \text{span}(\boldsymbol{\xi})$, it is sufficient to prove (39) for $\tilde{\boldsymbol{\tau}}_h = \boldsymbol{\xi}$. Re-
 242 calling that $\hat{\Pi}_{1,E}^0 \boldsymbol{\xi} \in \nabla \mathbb{P}_2^H(E)$, see (17), from (18), we have

$$\left\| \hat{\Pi}_{1,E}^0 \boldsymbol{\xi} \right\|_0 = \sup_{\mathbf{q} \in \nabla \mathbb{P}_2^H(E)} \frac{\left(\hat{\Pi}_{1,E}^0 \boldsymbol{\xi}, \mathbf{q} \right)}{\|\mathbf{q}\|_0} = \sup_{\mathbf{q} \in \nabla \mathbb{P}_2^H(E)} \frac{(\boldsymbol{\xi}, \mathbf{q})}{\|\mathbf{q}\|_0}. \quad (40)$$

By Varignon's theorem [31], for each element $E \in \mathcal{M}_h$, the quadrilateral K_E whose vertices are the edge midpoints M_j ($j = 1, \dots, 4$) of E , is a parallelogram. With the identification $V_5 = V_1$ we have

$$M_j = \frac{V_j + V_{j+1}}{2},$$

243 and the area of K_E satisfies $|K_E| = \frac{|E|}{2}$. Under the mesh assumptions **A.1**
 244 and **A.2**, it is not hard to show that the parallelogram is not degenerate,
 245 i.e. assumptions **A.1** and **A.2** hold true for K_E as well. We now construct
 246 $p^* \in \mathbb{P}_2^H(E)$ such that

$$p^*(M_j) = (-1)^j, \quad \text{for each } j = 1, \dots, 4. \quad (41)$$

To this aim, it is useful to resort to complex numbers $z = x + iy$. Hence, up to a translation, we can identify M_1 as $0 \in \mathbb{C}$; accordingly, we also set $M_2 = z_1$, $M_4 = z_2$ and $M_3 = z_1 + z_2$. A direct computation shows that the complex-valued polynomial

$$q(z) = -1 + 2 \frac{z_1 + z_2}{z_1 z_2} z - \frac{2}{z_1 z_2} z^2$$

247 satisfies conditions (41) (with the above-mentioned identifications of M_j).
 248 We now set $p^*(x, y) = \text{Re}(q(z))$, where $z = x + iy$ and $\text{Re}(\cdot)$ denotes the real
 249 part. The real-valued polynomial p^* is harmonic and satisfies conditions (41)
 250 as well. Let $\mathbf{p}^* := \nabla p^*$; from (40) we get

$$\left\| \hat{\Pi}_{1,E}^0 \boldsymbol{\xi} \right\|_0 \geq \frac{(\boldsymbol{\xi}, \mathbf{p}^*)}{\|\mathbf{p}^*\|_0}. \quad (42)$$

251 By an explicit computation using Cavalieri-Simpson's quadrature rule and

252 (41), we have that

$$\begin{aligned}
(\boldsymbol{\xi}, \mathbf{p}^*) &= \int_E \boldsymbol{\xi} \cdot \nabla p^* \, dE = \int_{\partial E} (\boldsymbol{\xi} \cdot \mathbf{n}) p^* \, de = \sum_{j=1}^4 \frac{(-1)^j}{|e_j|} \int_{e_j} p^* \, de \\
&= \sum_{j=1}^4 \frac{(-1)^j}{6} (p^*(V_j) + 4p^*(M_j) + p^*(V_{j+1})) \\
&= \sum_{j=1}^4 \frac{2}{3} (-1)^j p^*(M_j) = \frac{8}{3}.
\end{aligned} \tag{43}$$

253 We now notice that, due to assumptions **A.1** and **A.2**, there exists $C_{\mathbf{p}^*} >$
254 0 , independent of h_E , such that $\|\mathbf{p}^*\|_0 = \|\nabla p^*\|_0 \leq C_{\mathbf{p}^*}$. Therefore, using
255 Lemma 1 we have

$$\left\| \hat{\Pi}_{1,E}^0 \boldsymbol{\xi} \right\|_0 \geq \frac{8}{3 \|\mathbf{p}^*\|_0} = \frac{8 \|\boldsymbol{\xi}\|_0}{3 \|\boldsymbol{\xi}\|_0 \|\mathbf{p}^*\|_0} \geq \frac{8}{3C_\xi C_{\mathbf{p}^*}} \|\boldsymbol{\xi}\|_0. \tag{44}$$

256 Then, (39) holds true with $C_* = \frac{8}{3C_\xi C_{\mathbf{p}^*}}$. □

257 4.1. Continuity and coercivity of the local bilinear form $a_h^E(\cdot, \cdot)$

258 In this section, applying the above preliminary results, in particular
259 Lemma 2, we prove the continuity and coercivity (on the divergence operator
260 kernel) of the local bilinear form $a_h^E(\cdot, \cdot)$ in the L^2 -norm.

261 **Theorem 1.** *Under the mesh assumptions **A.1** and **A.2**, for every $E \in$*
262 *\mathcal{M}_h , the discrete bilinear form $a_h^E(\cdot, \cdot)$, defined in (20), is L^2 continuous and*
263 *coercive-on-the kernel, namely there exist two positive constants α_* and α^* ,*
264 *independent of h_E , such that*

$$a_h^E(\boldsymbol{\tau}_h, \boldsymbol{\sigma}_h) \leq \alpha^* \|\boldsymbol{\tau}_h\|_0 \|\boldsymbol{\sigma}_h\|_0 \quad \forall \boldsymbol{\tau}_h, \boldsymbol{\sigma}_h \in \Sigma_h(E) \tag{45}$$

265 and

$$a_h^E(\boldsymbol{\tau}_h, \boldsymbol{\tau}_h) \geq \alpha_* \|\boldsymbol{\tau}_h\|_0^2 \quad \forall \boldsymbol{\tau}_h \in \Sigma_h^0(E), \tag{46}$$

266 where Σ_h^0 is the divergence-free subspace defined in (30).

267 *Proof.* Fixed an element $E \in \mathcal{M}_h$, we first check the continuity. For every
268 $\boldsymbol{\tau}_h, \boldsymbol{\sigma}_h \in \Sigma_h(E)$, applying the definition of $\hat{\Pi}_E^0$, its continuity and the Cauchy-
269 Schwarz inequality, we obviously obtain

$$a_h^E(\boldsymbol{\tau}_h, \boldsymbol{\sigma}_h) = (\hat{\Pi}_{1,E}^0 \boldsymbol{\tau}_h, \hat{\Pi}_{1,E}^0 \boldsymbol{\sigma}_h) \leq \|\boldsymbol{\tau}_h\|_0 \|\boldsymbol{\sigma}_h\|_0. \tag{47}$$

270 Then (45) holds true with $\alpha^* = 1$.

Now, we prove the Σ_h^0 -coercivity of the bilinear form $a_h^E(\cdot, \cdot)$. From Proposition 1, we get that every $\boldsymbol{\tau}_h \in \Sigma_h^0$ can be written by means of the orthogonal decomposition

$$\boldsymbol{\tau}_h = \boldsymbol{\tau}_0 + \tilde{\boldsymbol{\tau}}_h,$$

where $\boldsymbol{\tau}_0 \in (\mathbb{P}_0(E))^2$ and $\tilde{\boldsymbol{\tau}}_h \in H(E)$. Moreover, one has

$$\|\boldsymbol{\tau}_h\|_0^2 = \|\boldsymbol{\tau}_0\|_0^2 + \|\tilde{\boldsymbol{\tau}}_h\|_0^2.$$

271 Using Lemma 2, the definition of the projection operator (18) and noticing
272 that $\hat{\Pi}_{1,E}^0 \boldsymbol{\tau}_0 = \boldsymbol{\tau}_0$, we have

$$\begin{aligned} a_h^E(\boldsymbol{\tau}_h, \boldsymbol{\tau}_h) &= \left(\hat{\Pi}_{1,E}^0 \boldsymbol{\tau}_h, \hat{\Pi}_{1,E}^0 \boldsymbol{\tau}_h \right) = \left(\hat{\Pi}_{1,E}^0 \boldsymbol{\tau}_0 + \hat{\Pi}_{1,E}^0 \tilde{\boldsymbol{\tau}}_h, \hat{\Pi}_{1,E}^0 \boldsymbol{\tau}_0 + \hat{\Pi}_{1,E}^0 \tilde{\boldsymbol{\tau}}_h \right) \\ &= (\boldsymbol{\tau}_0, \boldsymbol{\tau}_0) + 2(\boldsymbol{\tau}_0, \tilde{\boldsymbol{\tau}}_h) + \left(\hat{\Pi}_{1,E}^0 \tilde{\boldsymbol{\tau}}_h, \hat{\Pi}_{1,E}^0 \tilde{\boldsymbol{\tau}}_h \right) \\ &= (\boldsymbol{\tau}_0, \boldsymbol{\tau}_0) + \left(\hat{\Pi}_{1,E}^0 \tilde{\boldsymbol{\tau}}_h, \hat{\Pi}_{1,E}^0 \tilde{\boldsymbol{\tau}}_h \right) \\ &\geq (\boldsymbol{\tau}_0, \boldsymbol{\tau}_0) + C_* (\tilde{\boldsymbol{\tau}}_h, \tilde{\boldsymbol{\tau}}_h) \\ &\geq \min\{1, C_*\} [\|\boldsymbol{\tau}_0\|_0^2 + \|\tilde{\boldsymbol{\tau}}_h\|_0^2] \\ &= C_* \|\boldsymbol{\tau}_h\|_0^2, \end{aligned} \tag{48}$$

273 which yields the thesis, with $\alpha_* = C_*$. \square

274 4.2. Ellipticity-on-the-kernel condition and inf-sup condition

275 In this section, we consider the two conditions, i.e. the coercivity of the
276 bilinear form $a_h^E(\cdot, \cdot)$ on the kernel of the mixed term and the LBB inf-sup
277 condition, that imply the well-posedness of the discrete problem (25).

278 Let us introduce the discrete kernel space given by

$$K_h := \{ \boldsymbol{\tau}_h \in \Sigma_h : (\operatorname{div} \boldsymbol{\tau}_h, v_h) = 0 \ \forall v_h \in U_h \}. \tag{49}$$

279 Notice that $\forall \boldsymbol{\tau}_h \in K_h$ we have that $\operatorname{div} \boldsymbol{\tau}_h = 0$, so that $\boldsymbol{\tau}_h|_E \in \Sigma_h^0$ and
280 $\|\boldsymbol{\tau}_h\|_\Sigma = \|\boldsymbol{\tau}_h\|_0$. Hence, applying the local coercivity property (46) stated
281 in Theorem 1 and the definition of the bilinear form $a_h(\cdot, \cdot)$ (24), we obtain
282 that $\exists C_* > 0$, independent of h , such that

$$a_h(\boldsymbol{\tau}_h, \boldsymbol{\tau}_h) \geq C_* \|\boldsymbol{\tau}_h\|_\Sigma^2 \quad \forall \boldsymbol{\tau}_h \in K_h. \tag{50}$$

283 Furthermore, the inf-sup condition, i.e. $\exists \beta > 0$, independent of h , such
 284 that

$$\inf_{v \in U_h} \sup_{\boldsymbol{\tau}_h \in \Sigma_h} \frac{(\operatorname{div} \boldsymbol{\tau}_h, v)_\Omega}{\|v\|_0 \|\boldsymbol{\tau}_h\|_\Sigma} \geq \beta \quad (51)$$

285 is a consequence of the so-called *Fortin's trick*, cf. [2], when the interpolation
 286 operator \mathcal{I}_h of Section 3.2 is considered (see in particular (10), (13) and (14)
 287 with $s = 0$).

288 5. Error estimates in the quadrilateral case

289 We prove optimal a priori error estimates for the method presented in
 290 this work, when the mesh is made up by quadrilaterals. We remark that the
 291 proof follows the usual guidelines for the VEM mixed schemes; however, we
 292 provide all the details, for the sake of completeness.

Theorem 2. *Let $(\boldsymbol{\sigma}, u) \in [\mathbf{H}^1(\Omega)]^2 \times \mathbf{H}_0^1(\Omega)$ and $f \in \mathbf{H}^1(\Omega)$ be respectively solution and forcing term of (2). Then $\exists C > 0$, independent of h , such that the unique solution $(\boldsymbol{\sigma}_h, u_h) \in \Sigma_h \times U_h$ of (25) satisfies the following error estimates:*

$$\|\boldsymbol{\sigma} - \boldsymbol{\sigma}_h\|_0 \leq Ch |\boldsymbol{\sigma}|_1, \quad (52)$$

$$\|\operatorname{div}(\boldsymbol{\sigma} - \boldsymbol{\sigma}_h)\|_0 \leq Ch |f|_1, \quad (53)$$

$$\|u - u_h\|_0 \leq Ch (|u|_1 + |\boldsymbol{\sigma}|_1). \quad (54)$$

293 *Proof.* In order to prove (52), let $\boldsymbol{\sigma}_I := \mathcal{I}_h \boldsymbol{\sigma} \in \Sigma_h$ be the interpolant of $\boldsymbol{\sigma}$
 294 defined in Section 3.2. Then, applying the triangle inequality we obtain

$$\|\boldsymbol{\sigma} - \boldsymbol{\sigma}_h\|_0 \leq \|\boldsymbol{\sigma} - \boldsymbol{\sigma}_I\|_0 + \|\boldsymbol{\sigma}_I - \boldsymbol{\sigma}_h\|_0. \quad (55)$$

295 Let us focus on the term $\|\boldsymbol{\sigma}_I - \boldsymbol{\sigma}_h\|_0$. Notice that, applying the second
 296 equation of discrete problem (25) and the property of the interpolant (11),
 297 we have for each $E \in \mathcal{M}_h$

$$\operatorname{div} \boldsymbol{\sigma}_h = -\Pi_{0,E}^0 f = \Pi_{0,E}^0 \operatorname{div} \boldsymbol{\sigma} = \operatorname{div} \boldsymbol{\sigma}_I \implies \operatorname{div}(\boldsymbol{\sigma}_I - \boldsymbol{\sigma}_h) = 0, \quad (56)$$

298 hence $(\boldsymbol{\sigma}_I - \boldsymbol{\sigma}_h)|_E \in \Sigma_h^0$ for each $E \in \mathcal{M}_h$ (therefore $(\boldsymbol{\sigma}_I - \boldsymbol{\sigma}_h) \in K_h$).
 299 Notice that applying this relation to the first equation of the discrete problem
 300 (25) and to the first equation of the continuous problem (2) we obtain that

301 $a_h(\boldsymbol{\sigma}_h, \boldsymbol{\sigma}_I - \boldsymbol{\sigma}_h) = 0$ and $a(\boldsymbol{\sigma}, \boldsymbol{\sigma}_I - \boldsymbol{\sigma}_h) = 0$. Then, since $\boldsymbol{\sigma}_I - \boldsymbol{\sigma}_h \in K_h$ we
 302 can apply Theorem (1), in particular (46), and obtain the estimate

$$\begin{aligned}
 \alpha_* \|\boldsymbol{\sigma}_I - \boldsymbol{\sigma}_h\|_0^2 &\leq a_h(\boldsymbol{\sigma}_I - \boldsymbol{\sigma}_h, \boldsymbol{\sigma}_I - \boldsymbol{\sigma}_h) \\
 &= a_h(\boldsymbol{\sigma}_I, \boldsymbol{\sigma}_I - \boldsymbol{\sigma}_h) \\
 &= \sum_{E \in \mathcal{M}_h} \left(a_h^E(\boldsymbol{\sigma}_I - \hat{\Pi}_{1,E}^0 \boldsymbol{\sigma}, \boldsymbol{\sigma}_I - \boldsymbol{\sigma}_h) + a_h^E(\hat{\Pi}_{1,E}^0 \boldsymbol{\sigma}, \boldsymbol{\sigma}_I - \boldsymbol{\sigma}_h) \right) \\
 &= \sum_{E \in \mathcal{M}_h} \left(a_h^E(\boldsymbol{\sigma}_I - \hat{\Pi}_{1,E}^0 \boldsymbol{\sigma}, \boldsymbol{\sigma}_I - \boldsymbol{\sigma}_h) + a^E(\hat{\Pi}_{1,E}^0 \boldsymbol{\sigma}, \boldsymbol{\sigma}_I - \boldsymbol{\sigma}_h) \right) \\
 &= \sum_{E \in \mathcal{M}_h} \left(a_h^E(\boldsymbol{\sigma}_I - \hat{\Pi}_{1,E}^0 \boldsymbol{\sigma}, \boldsymbol{\sigma}_I - \boldsymbol{\sigma}_h) + a^E(\hat{\Pi}_{1,E}^0 \boldsymbol{\sigma} - \boldsymbol{\sigma}, \boldsymbol{\sigma}_I - \boldsymbol{\sigma}_h) \right),
 \end{aligned} \tag{57}$$

303 where the projector $\hat{\Pi}_{1,E}^0$ is defined by the orthogonality condition (18) and
 304 satisfies, for each $E \in \mathcal{M}_h$, $a_h^E(\hat{\Pi}_{1,E}^0 \boldsymbol{\sigma}, \boldsymbol{\tau}_h) = a^E(\hat{\Pi}_{1,E}^0 \boldsymbol{\sigma}, \boldsymbol{\tau}_h) \forall \boldsymbol{\tau}_h \in \Sigma_h$. We
 305 now notice that, since $\boldsymbol{\sigma} = \nabla u$ and $\hat{\Pi}_{1,E}^0$ projects onto the space $\nabla \mathbb{P}_2^H(E)$, it
 306 holds

$$\left\| \boldsymbol{\sigma} - \hat{\Pi}_{1,E}^0 \boldsymbol{\sigma} \right\|_{0,E} = \left\| \nabla u - \hat{\Pi}_{1,E}^0(\nabla u) \right\|_{0,E} = \inf_{p \in \mathbb{P}_2^H(E)} |u - p|_{1,E} \leq Ch_E |\boldsymbol{\sigma}|_{1,E}, \tag{58}$$

307 where the last estimate follows from the standard approximation theory,
 308 see [32, 33, 34]. Then, by the continuity of $a_h^E(\cdot, \cdot)$ and $a^E(\cdot, \cdot)$, applying
 309 estimates (15) and (58), we obtain

$$\begin{aligned}
 \|\boldsymbol{\sigma}_I - \boldsymbol{\sigma}_h\|_0 &\leq C \sum_{E \in \mathcal{M}_h} \left(\left\| \boldsymbol{\sigma}_I - \hat{\Pi}_{1,E}^0 \boldsymbol{\sigma} \right\|_{0,E} + \left\| \boldsymbol{\sigma} - \hat{\Pi}_{1,E}^0 \boldsymbol{\sigma} \right\|_{0,E} \right) \\
 &\leq C \left(\|\boldsymbol{\sigma} - \boldsymbol{\sigma}_I\|_0 + \sum_{E \in \mathcal{M}_h} \left\| \boldsymbol{\sigma} - \hat{\Pi}_{1,E}^0 \boldsymbol{\sigma} \right\|_{0,E} \right) \\
 &\leq Ch |\boldsymbol{\sigma}|_1.
 \end{aligned} \tag{59}$$

310 Applying this relation and the interpolation estimate (15) to (55), estimate
 311 (52) is proved. Moreover, to prove (53) we apply (56), the interpolation
 312 estimate (14) and the equation $\operatorname{div} \boldsymbol{\sigma} = -f$, to obtain

$$\|\operatorname{div} \boldsymbol{\sigma} - \operatorname{div} \boldsymbol{\sigma}_h\|_0 \leq \|\operatorname{div} \boldsymbol{\sigma} - \operatorname{div} \boldsymbol{\sigma}_I\|_0 \leq Ch |f|_1. \tag{60}$$

313 Finally, we have to prove (54). Let $u_I := \Pi_{0,h}^0 u \in U_h$. Notice that by its
 314 definition u_I satisfies $(u - u_I, \operatorname{div} \boldsymbol{\tau}_h)_\Omega = 0$ for each $\boldsymbol{\tau}_h \in \Sigma_h$. By triangle
 315 inequality we have

$$\|u - u_h\|_0 \leq \|u - u_I\|_0 + \|u_I - u_h\|_0. \quad (61)$$

316 First, let us consider the term $\|u_I - u_h\|_0$. Since $u_I - u_h \in U_h$, according to
 317 the inf-sup condition (51), there exists $\boldsymbol{\tau}_h^* \in \Sigma_h$ be such that $\operatorname{div} \boldsymbol{\tau}_h^* = u_I - u_h$
 318 and

$$\|\boldsymbol{\tau}_h^*\|_0 \leq \frac{1}{\beta} \|u_I - u_h\|_0. \quad (62)$$

319 Then, applying the continuous problem (2), the discrete one (25) and adding
 320 and subtracting $\hat{\Pi}_E^0 \boldsymbol{\sigma}$, we obtain

$$\begin{aligned} \|u_I - u_h\|_0^2 &= (u_I - u_h, \operatorname{div} \boldsymbol{\tau}_h^*)_\Omega \\ &= (u - u_h, \operatorname{div} \boldsymbol{\tau}_h^*)_\Omega \\ &= a(\boldsymbol{\sigma}, \boldsymbol{\tau}_h^*) - a_h(\boldsymbol{\sigma}_h, \boldsymbol{\tau}_h^*) \\ &= \sum_{E \in \mathcal{M}_h} a^E \left(\boldsymbol{\sigma} - \hat{\Pi}_{1,E}^0 \boldsymbol{\sigma}, \boldsymbol{\tau}_h^* \right) + a_h^E \left(\hat{\Pi}_{1,E}^0 \boldsymbol{\sigma} - \boldsymbol{\sigma}_h, \boldsymbol{\tau}_h^* \right) \\ &\leq C \sum_{E \in \mathcal{M}_h} \left(\left\| \boldsymbol{\sigma} - \hat{\Pi}_{1,E}^0 \boldsymbol{\sigma} \right\|_{0,E} + \|\boldsymbol{\sigma} - \boldsymbol{\sigma}_h\|_{0,E} \right) \|u_I - u_h\|_0 \end{aligned} \quad (63)$$

321 where in the last step we exploit the continuity of the bilinear forms together
 322 with (62). Finally, applying (63) to (61), the interpolation estimate (16) and
 323 the error estimate of $\boldsymbol{\sigma}$ (52) already proved, we obtain

$$\begin{aligned} \|u - u_h\|_0 &\leq \|u - u_I\|_0 + C \left(\sum_{E \in \mathcal{M}_h} \left\| \boldsymbol{\sigma} - \hat{\Pi}_{1,E}^0 \boldsymbol{\sigma} \right\|_{0,E} + \|\boldsymbol{\sigma} - \boldsymbol{\sigma}_h\|_0 \right) \\ &\leq Ch (|u|_1 + |\boldsymbol{\sigma}|_1). \end{aligned} \quad (64)$$

324

□

325 6. Numerical Tests

326 6.1. Convergence tests

In this section, we numerically assess the behaviour of our scheme with respect to mesh refinement. We consider $\Omega = (0, 1)^2$ and solve Problem (25)

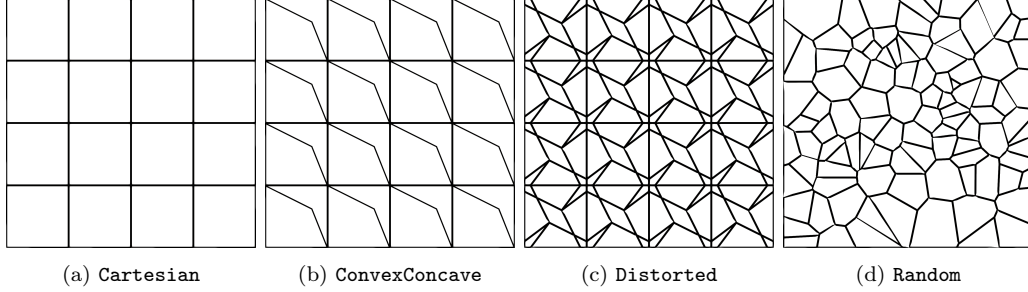


Figure 2: Meshes.

choosing f such that

$$u(x, y) = x(1 - x)y(1 - y),$$

$$\boldsymbol{\sigma}(x, y) = \nabla u(x, y) = \begin{pmatrix} (1 - 2x)y(1 - y) \\ x(1 - x)(1 - 2y) \end{pmatrix}.$$

First, we consider the four families of meshes depicted in Figure 2. We assess the method behaviour by computing the following relative errors:

$$\text{err}_u = \frac{1}{\|u\|_0} \left(\sum_{E \in \mathcal{M}_h} \|u - u_h\|_{0,E}^2 \right)^{\frac{1}{2}},$$

$$\text{err}_{\text{div}} = \frac{1}{\|\text{div } \boldsymbol{\sigma}\|_0} \sum_{E \in \mathcal{M}_h} \left(\|\text{div } \boldsymbol{\sigma} - \text{div } \boldsymbol{\sigma}_h\|_{0,E}^2 \right)^{\frac{1}{2}},$$

$$\text{err}_{\boldsymbol{\sigma}} = \frac{1}{\|\boldsymbol{\sigma}\|_0} \left(\sum_{E \in \mathcal{M}_h} \left\| \boldsymbol{\sigma} - \hat{\Pi}_{k-1,E}^0 \boldsymbol{\sigma}_h \right\|_{0,E}^2 \right)^{\frac{1}{2}},$$

$$\text{err}_{\boldsymbol{\sigma} \cdot \mathbf{n}} = \frac{\left(\sum_{e \in \mathcal{E}_h} h_e \|(\boldsymbol{\sigma} - \boldsymbol{\sigma}_h) \cdot \mathbf{n}^e\|_{0,e} \right)^{\frac{1}{2}}}{\left(\sum_{e \in \mathcal{E}_h} h_e \|\boldsymbol{\sigma} \cdot \mathbf{n}^e\|_{0,e} \right)^{\frac{1}{2}}},$$

327 where \mathcal{E}_h denotes the set all edges of \mathcal{M}_h . We also solve the test problem
 328 with the mixed finite element $RT_0 - P_0$ [2], and the standard VEM method
 329 [4]. We recall that for this latter method, the local discrete bilinear form
 330 $a_h(\cdot, \cdot)$ is given by

$$a_h^E(\boldsymbol{\sigma}_h, \boldsymbol{\tau}_h) = (\Pi_{0,E}^0 \boldsymbol{\sigma}_h, \Pi_{0,E}^0 \boldsymbol{\tau}_h)_E + s^E ((I - \Pi_{0,E}^0) \boldsymbol{\sigma}_h, (I - \Pi_{0,E}^0) \boldsymbol{\tau}_h), \quad (65)$$

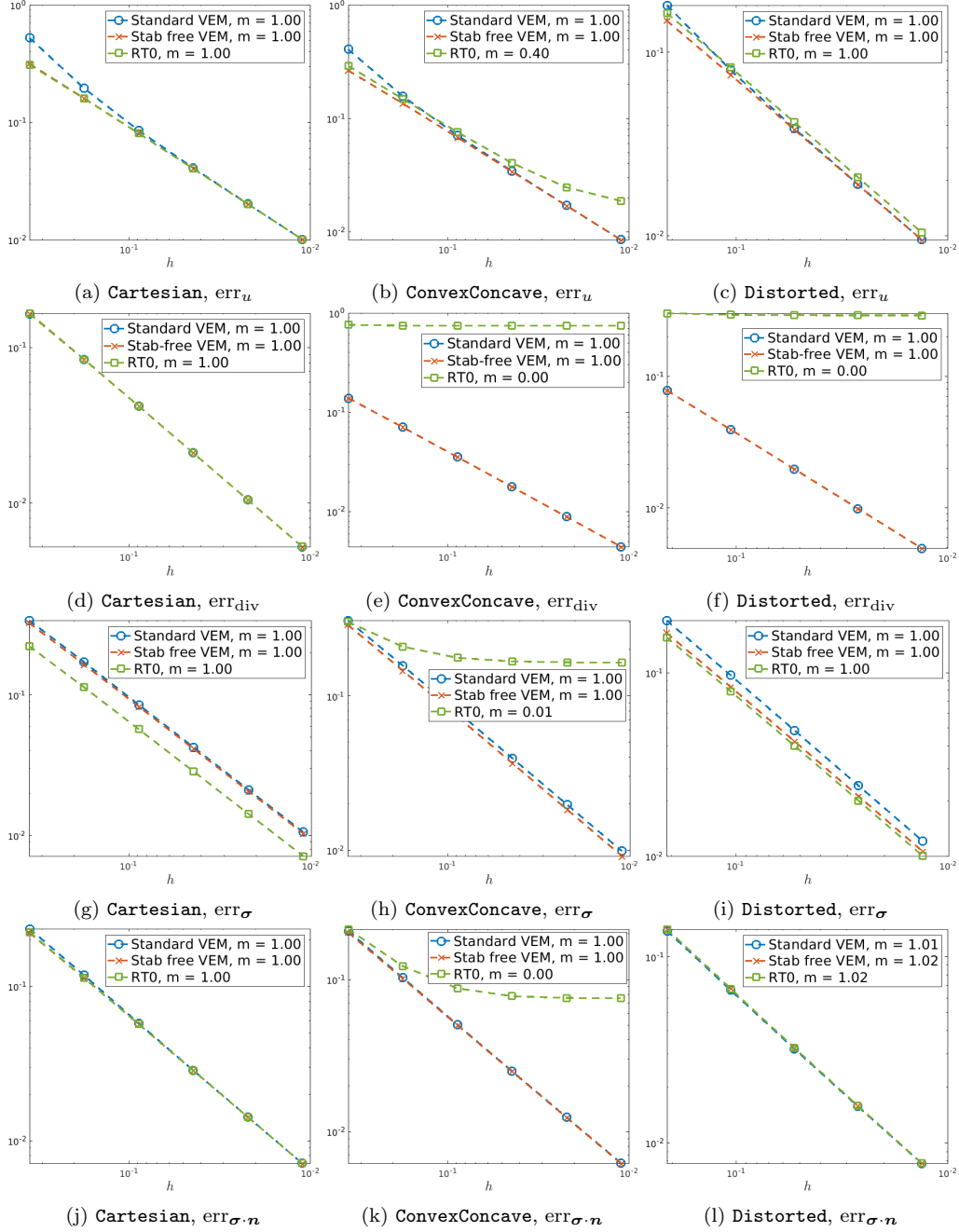


Figure 3: Convergence curves on quadrilateral meshes. The vertical axis refers to the values of the errors.

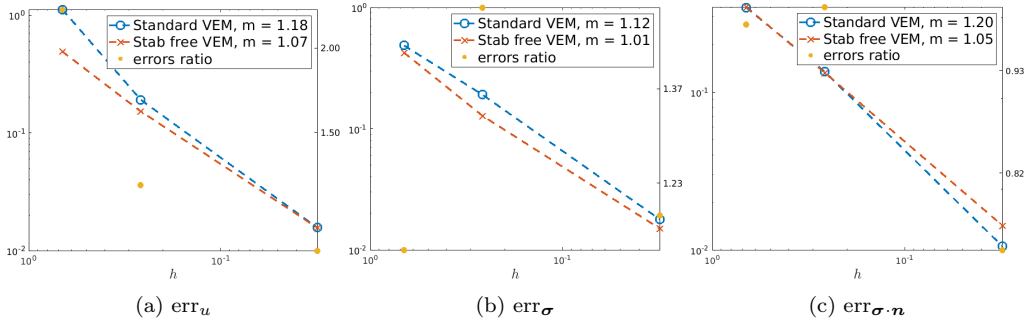


Figure 4: Convergence curves on **Random** mesh. The left vertical axis refers to the values of the errors (*dotted lines*). The right vertical axis refers to the ratio between the error made by the standard VEM method and the error of the proposed method (*orange dots*).

331 where $s^E(\cdot, \cdot)$ is the local stabilization term. In matrix form, the stabilization
 332 term we choose is given by

$$\mathbf{S} = (\mathbf{I} - \mathbf{\Pi}^0)^T \mathbf{D} (\mathbf{I} - \mathbf{\Pi}^0), \quad (66)$$

333 where the matrix $\mathbf{\Pi}^0$ represents the projection onto the constant vector func-
 334 tions. Moreover, \mathbf{D} is a diagonal matrix defined as

$$\mathbf{D}_{ii} = \max \left(h_E |e_i|, (\Pi_{0,E}^0 \varphi_i, \Pi_{0,E}^0 \varphi_i)_E \right). \quad (67)$$

335 Above, the functions φ_i denote the elements of the Lagrangian basis corre-
 336 sponding to the local degrees of freedom (4). This choice is known as D-recipe
 337 stabilization, and it is inspired by the numerical assessment in [18, 19]. We
 338 also notice that in computing the error err_σ , for the standard VEM we use
 339 the projection onto constants.

340 In Figure 3, we consider the quadrilateral meshes of Figures 2a, 2b and
 341 2c, respectively named **Cartesian**, **ConvexConcave** and **Distorted**. The
 342 computed errors obtained by the three methods are compared with respect
 343 to the maximum diameter of the mesh, denoted by h , and the asymptotical
 344 convergence rates (m) are reported in the legend. The results show that
 345 the two VE methods behave equivalently on all meshes concerning all the
 346 computed errors, whereas the mixed FE method has a similar behavior to
 347 VE methods just on **Cartesian** mesh. Indeed, it is well-known that the
 348 Piola transformation corresponding to the mapping from the square parent
 349 element to a physical one, is a diffeomorphism only for convex elements.
 350 This is the reason why the FE method does not converge on **ConvexConcave**

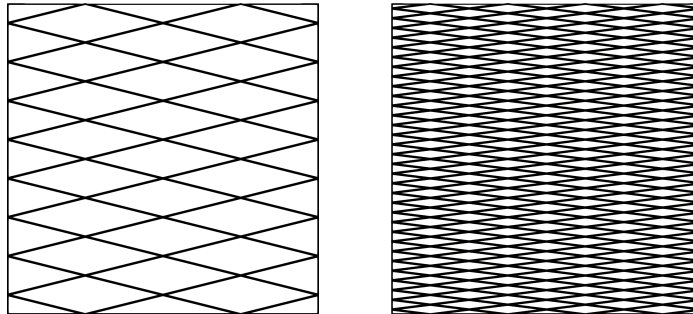


Figure 5: Rhomboidal mesh: anisotropic h-refinement

351 mesh. Instead, as far as the `Distorted` mesh is concerned, it is known
 352 that the err_{div} does not converge for the Raviart-Thomas Finite Element
 353 on general shape-regular, though convex, quadrilaterals (see [35] for more
 354 details). We also remark that on all the meshes, both the VEM methods
 355 return exactly the same results for err_{div} . This is not surprising, since for all
 356 the meshes and both the VEM methods, from the second equation of (25)
 357 we get $\text{div } \boldsymbol{\sigma}_h = -\Pi_{0,E}^0 f$, while $\text{div } \boldsymbol{\sigma} = -f$. Hence err_{div} is always the L^2
 358 error when the load term f is approximated by piecewise constant functions.
 359 Accordingly, from now on we will not display that error quantity.

360 In Figure 2d we consider the family of meshes named `Random`, i.e. polyg-
 361 onal meshes obtained using *Polymesher* [36], whose elements are not only
 362 quadrilaterals. On each polygon, we construct the local bilinear form $a_h^E(\cdot, \cdot)$
 363 (20) choosing k as in (19) (see Remark 1). As we can see in Figure 4, the
 364 proposed method is stable and exhibits the expected convergence rates.

365 6.2. Comparison with standard VEM on an anisotropic refinement test

366 In this section, we consider the problem presented in the previous section
 367 with a `Rhomboidal` mesh, as depicted in Figure 5. This mesh is refined
 368 applying an anisotropic rule. In particular, at each step the mesh is refined
 369 by a factor α in the x-direction and by a factor α^2 in the y-direction. In Figure
 370 6, we present the convergence plots. We observe that both the mixed finite
 371 element method and the standard VEM method are not properly converging,
 372 while the proposed scheme exhibits the expected convergence behaviour.

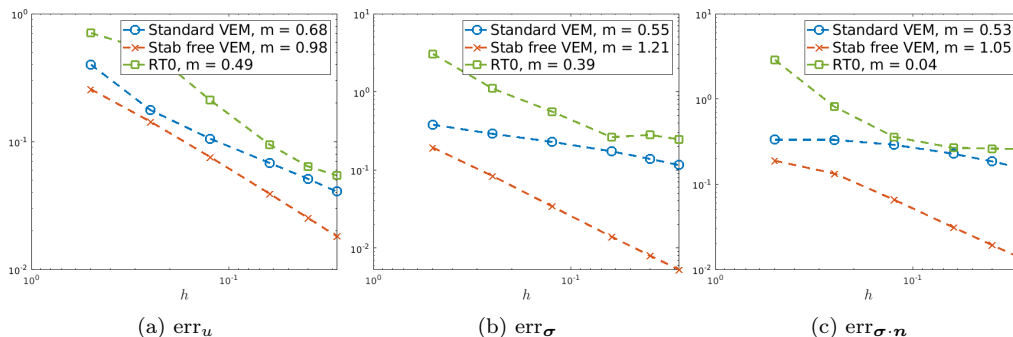


Figure 6: Convergence curves on Rhomboidal mesh. The vertical axis refers to the values of the errors.

373 7. Conclusions

374 We have presented a self-stabilized Virtual Element Method for the Pois-
 375 son problem in mixed form. One of the main features of our approach is
 376 the use of a projection operator over the gradients of harmonic polynomi-
 377 als of suitable degree. This choice alleviates the computational costs arising
 378 from the numerical quadrature. Despite the scheme is designed for arbitrary
 379 polygons, the theoretical analysis has been developed only for quadrilateral
 380 meshes. The method convergence and stability have been computationally
 381 confirmed. Moreover, the numerical results show that our scheme is a valid
 382 alternative to the standard lowest-order mixed VEM.

383 A possible future development of the present study is the extension of the
 384 analysis to general polygonal meshes.

385 Acknowledgements

386 The authors kindly acknowledge partial financial support by INdAM-
 387 GNCS projects 2022 CUP_E55F2200027001. C.L. and M.V. kindly ac-
 388 knowledge partial financial support by PRIN 2017 (No. 201744KLJL) and
 389 PRIN 2020 (No. 20204LN5N5), funded by the Italian Ministry of Universi-
 390 ties and Research (MUR). A.B and F.M. kindly acknowledge financial sup-
 391 port provided by PNRR M4C2 project of CN00000013 National Centre for
 392 HPC, Big Data and Quantum Computing (HPC) CUP:E13C22000990001.
 393 A.B. kindly acknowledges partial financial support provided by INdAM-
 394 GNCS Projects 2023, MIUR project “Dipartimenti di Eccellenza” Programme

395 (2018–2022) CUP:E11G18000350001 and by the PRIN 2020 project (No.
396 20204LN5N5_003).

397 **References**

- 398 [1] L. Beirão da Veiga, F. Brezzi, A. Cangiani, G. Manzini, L. D. Marini,
399 A. Russo, Basic principles of virtual element methods, *Mathematical*
400 *Models and Methods in Applied Sciences* 23 (01) (2013) 199–214. doi:
401 10.1142/S0218202512500492.
- 402 [2] D. Boffi, F. Brezzi, M. Fortin, *Mixed Finite Element Methods and Ap-*
403 *plications*, Springer Berlin Heidelberg, 2013. doi:[https://doi.org/](https://doi.org/10.1007/978-3-642-36519-5)
404 10.1007/978-3-642-36519-5.
- 405 [3] F. Brezzi, R. S. Falk, L. D. Marini, Basic principles of mixed virtual el-
406 ement methods, *ESAIM: Mathematical Modelling and Numerical Anal-*
407 *ysis* 48 (4) (2014) 1227–1240. doi:10.1051/m2an/2013138.
- 408 [4] L. Beirão da Veiga, F. Brezzi, L. D. Marini, A. Russo, Mixed virtual
409 element methods for general second order elliptic problems on polygonal
410 meshes, *ESAIM: Mathematical Modelling and Numerical Analysis* 50 (3)
411 (2016) 727–747. doi:10.1051/m2an/2015067.
- 412 [5] L. Beirão da Veiga, F. Brezzi, L. D. Marini, A. Russo, $H(\text{div})$ and
413 $H(\text{curl})$ -conforming virtual element methods, *Numerische Mathematik*
414 133 (2) (2016) 303–332. doi:10.1007/s00211-015-0746-1.
- 415 [6] F. Dassi, G. Vacca, Bricks for the mixed high-order virtual element
416 method: Projectors and differential operators, *Applied Numerical*
417 *Mathematics* 155 (2020) 140–159. doi:[https://doi.org/10.1016/j.](https://doi.org/10.1016/j.apnum.2019.03.014)
418 [apnum.2019.03.014](https://doi.org/10.1016/j.apnum.2019.03.014).
- 419 [7] L. Beirão da Veiga, C. Lovadina, D. Mora, A virtual element method for
420 elastic and inelastic problems on polytope meshes, *Computer Methods*
421 *in Applied Mechanics and Engineering* 295 (2015) 327–346. doi:10.
422 1016/j.cma.2015.07.013.
- 423 [8] E. Artioli, S. de Miranda, C. Lovadina, L. Patruno, A
424 stress/displacement virtual element method for plane elasticity prob-
425 lems, *Computer Methods in Applied Mechanics and Engineering* 325
426 (2017) 155–174. doi:<https://doi.org/10.1016/j.cma.2017.06.036>.

- 427 [9] F. Dassi, C. Lovadina, M. Visinoni, A three-dimensional
428 Hellinger–Reissner virtual element method for linear elasticity prob-
429 lems, *Computer Methods in Applied Mechanics and Engineering* 364
430 (2020) 112910. doi:<https://doi.org/10.1016/j.cma.2020.112910>.
- 431 [10] F. Dassi, C. Lovadina, M. Visinoni, Hybridization of the virtual ele-
432 ment method for linear elasticity problems, *Mathematical Models and*
433 *Methods in Applied Sciences* 31 (14) (2021) 2979–3008. doi:[10.1142/
434 S0218202521500676](https://doi.org/10.1142/S0218202521500676).
- 435 [11] M. F. Benedetto, S. Berrone, A. Borio, The Virtual Element Method
436 for underground flow simulations in fractured media, in: *Advances*
437 *in Discretization Methods*, Vol. 12 of SEMA SIMAI Springer Series,
438 Springer International Publishing, Switzerland, 2016, pp. 167–186. doi:
439 [10.1007/978-3-319-41246-7_8](https://doi.org/10.1007/978-3-319-41246-7_8).
- 440 [12] M. F. Benedetto, S. Berrone, A. Borio, S. Pieraccini, S. Scialò, A hybrid
441 mortar virtual element method for discrete fracture network simulations,
442 *Journal of Computational Physics* 306 (2016) 148–166. doi:[10.1016/
443 j.jcp.2015.11.034](https://doi.org/10.1016/j.jcp.2015.11.034).
- 444 [13] M. Benedetto, A. Borio, F. Kyburg, J. Mollica, S. Scialò, An arbitrary
445 order mixed virtual element formulation for coupled multi-dimensional
446 flow problems, *Computer Methods in Applied Mechanics and Engineer-*
447 *ing* 391 (2022) 114204. doi:[10.1016/j.cma.2021.114204](https://doi.org/10.1016/j.cma.2021.114204).
448 URL [https://www.sciencedirect.com/science/article/pii/
449 S0045782521005351](https://www.sciencedirect.com/science/article/pii/S0045782521005351)
- 450 [14] S. Berrone, M. Busetto, F. Vicini, Virtual element simulation of two-
451 phase flow of immiscible fluids in discrete fracture networks, *Journal of*
452 *Computational Physics* 473 (2023) 111735. doi:[https://doi.org/10.
453 1016/j.jcp.2022.111735](https://doi.org/10.1016/j.jcp.2022.111735).
- 454 [15] A. Borio, F. P. Hamon, N. Castelletto, J. A. White, R. R. Settghost, Hy-
455 brid mimetic finite-difference and virtual element formulation for cou-
456 pled poromechanics, *Computer Methods in Applied Mechanics and En-*
457 *gineering* 383 (2021) 113917. doi:[https://doi.org/10.1016/j.cma.
458 2021.113917](https://doi.org/10.1016/j.cma.2021.113917).

- 459 [16] S. Berrone, A. Borio, A. D’Auria, S. Scialò, F. Vicini, A robust vem-
460 based approach for flow simulations in poro-fractured media, *Mathemat-*
461 *ical Models and Methods in Applied Sciences* 31 (14) (2021) 2855–2885.
462 doi:10.1142/S0218202521500639.
- 463 [17] S. Berrone, M. Busetto, A virtual element method for the two-
464 phase flow of immiscible fluids in porous media, *Computational*
465 *Geosciences* 26 (2022) 195–216. doi:https://doi.org/10.1007/
466 s10596-021-10116-4.
- 467 [18] L. Beirão da Veiga, F. Dassi, A. Russo, High-order virtual element
468 method on polyhedral meshes, *Computers and Mathematics with Ap-*
469 *plications* 74 (2017).
- 470 [19] F. Dassi, L. Mascotto, Exploring high-order three dimensional virtual
471 elements: Bases and stabilizations, *Computers and Mathematics with*
472 *Applications* 75 (2018).
- 473 [20] A. Cangiani, E. H. Georgoulis, T. Pryer, O. J. Sutton, A posteriori
474 error estimates for the virtual element method, *Numerische Mathematik*
475 137 (4) (2017) 857–893. doi:10.1007/s00211-017-0891-9.
- 476 [21] S. Berrone, A. Borio, A residual a posteriori error estimate for the virtual
477 element method, *Mathematical Models and Methods in Applied Sciences*
478 27 (08) (2017) 1423–1458. doi:10.1142/S0218202517500233.
- 479 [22] L. Beirão da Veiga, C. Canuto, R. H. Nochetto, G. Vacca, M. Verani,
480 Adaptive VEM: Stabilization-free a posteriori error analysis and contrac-
481 tion property, arXiv:2111.07656 (2021). doi:10.48550/ARXIV.2111.
482 07656.
- 483 [23] S. Berrone, A. Borio, F. Marcon, Lowest order stabilization free Vir-
484 tual Element Method for the Poisson equation, arXiv:2103.16896 (2021).
485 arXiv:2103.16896.
- 486 [24] S. Berrone, A. Borio, F. Marcon, Comparison of standard and stabi-
487 lization free Virtual Elements on anisotropic elliptic problems, *Applied*
488 *Mathematics Letters* 129 (2022) 107971. doi:10.1016/j.aml.2022.
489 107971.

- 490 [25] A. D’Altri, S. de Miranda, L. Patruno, E. Sacco, An enhanced vem for-
491 mulation for plane elasticity, *Computer Methods in Applied Mechanics*
492 and *Engineering* 376 (2021) 113663. doi:[https://doi.org/10.1016/
493 j.cma.2020.113663](https://doi.org/10.1016/j.cma.2020.113663).
- 494 [26] A. Lamperti, M. Cremonesi, U. Perego, C. Lovadina, A. Russo, A Hu-
495 Washizu variational approach to self-stabilized Virtual Elements: 2D
496 linear elastostatics, *Computational Mechanics* 71 (2023) 935–955.
- 497 [27] A. Chen, N. Sukumar, Stabilization-free serendipity virtual element
498 method for plane elasticity, *Computer Methods in Applied Mechanics*
499 and *Engineering* 404 (2023) 115784.
- 500 [28] A. Chen, N. Sukumar, Stabilization-free virtual element method for
501 plane elasticity, *Computers and Mathematics with Applications* 138
502 (2023) 88–105.
- 503 [29] S. Berrone, A. Borio, F. Marcon, G. Teora, A first-order stabilization-
504 free virtual element method, *Applied Mathematics Letters* 142 (2023)
505 108641. doi:<https://doi.org/10.1016/j.aml.2023.108641>.
- 506 [30] A. Sommariva, M. Vianello, Product Gauss cubature over polygons
507 based on Green’s integration formula, *BIT Numerical Mathematics*
508 47 (2) (2007) 441 – 453. doi:[10.1007/s10543-007-0131-2](https://doi.org/10.1007/s10543-007-0131-2).
- 509 [31] H. S. M. Coxeter, S. L. Greitzer, *Geometry revisited*, 1st Edition, Vol. 19
510 of Anneli Lax New Mathematical Library, Random House, New York,
511 1967.
- 512 [32] J. H. Bramble, S. R. Hilbert, Estimation of linear functionals on Sobolev
513 spaces with application to fourier transforms and spline interpolation,
514 *SIAM journal on numerical analysis* 7 (1) (1970) 112–124.
- 515 [33] T. Dupont, L. R. Scott, Polynomial approximation of functions in
516 sobolev spaces, *Mathematics of computation* 34 (150) (1980) 441–463.
- 517 [34] S. C. Brenner, L. R. Scott, *The mathematical theory of finite ele-
518 ment methods*, 3rd Edition, Vol. 15 of Texts in Applied Mathematics,
519 Springer, New York, 2008.

- 520 [35] D. N. Arnold, D. Boffi, R. S. Falk, Quadrilateral $H(\text{div})$ finite elements,
521 SIAM Journal on Numerical Analysis 42 (6) (2005) 2429–2451.
- 522 [36] C. Talischi, G. H. Paulino, A. Pereira, I. F. M. Menezes, Polymesher:
523 A general-purpose mesh generator for polygonal elements written in
524 matlab, Struct. Multidiscipl. Optim. 45 (3) (2012) 309–328. doi:
525 10.1007/s00158-011-0706-z.